American Mineralogist, Volume 67, pages 251–268, 1982

Use of exsolution lamellae in lunar clinopyroxenes as cooling rate speedometers: an experimental calibration

TIMOTHY L. GROVE

Department of Earth and Planetary Sciences
Massachusetts Institute of Technology
Cambridge, Massachusetts 02139

Abstract

Clinopyroxenes in Apollo 15 quartz-normative basalts (QNBs) are chemically complex recorders of thermal history. Texturally distinctive augite rims ($Wo_{30}En_{42}$) mantle the clinopyroxene phenocrysts and contain submicroscopic exsolution lamellae of pigeonite and augite near the (001) and (100) orientations. The size and morphologic variations of exsolution textures were characterized using the transmission electron microscope (TEM) in cooling rate experiments (cooled over the range 0.21° to 150°C/hr) on a synthetic QNB composition and in lunar samples 15597, 15499 and 15058. The size variation of (001) exsolution lamellae is used to estimate the sample's thermal history. The lamellae coarsen over the temperature interval 1100°–800°C, record cooling rate over this temperature range and may be used as cooling rate speedometers. Augite–pigeonite intergrowths form by spinodal decomposition, homogeneous nucleation, and heterogeneous nucleation. Coarsening of the lamellae produced in the cooling rate experiments may be described by the rate law:

$$\lambda = \lambda^\circ + kt^{1/3}$$

where $\lambda^\circ = 70$Å, $k = 107.3$ and t is time in days. Thermal histories of lunar basalts 15597, 15499 and 15058 estimated with the lamellae coarsening speedometer are comparable to those estimated from grain size.

In the Apollo 15 QNBs three lamellar orientations dominate; (100) and two sets of (001). Heterogeneously nucleated (100) and (001) lamellae grow with $C2/c$ symmetry, but the homogeneously nucleated (001) lamellae grow as coexisting $C2/c$ and $P2_1/c$. All orientations form over a restricted temperature (1100–1066°C) but have different orientations as a consequence of the change in cell dimensions that occurs during the $C2/c$ to $P2_1/c$ transition.

Introduction

Transmission electron microscope (TEM) observations have revealed a variety of submicroscopic textures in lunar (Radcliffe *et al.*, 1970; Christie *et al.*, 1971; Lally *et al.*, 1975) and terrestrial (Dunham *et al.*, 1972; Copley *et al.*, 1974) pyroxenes that are related to order/disorder transformations and exsolution reactions. Examination of pyroxenes from samples which had experienced differing cooling histories led to the discovery of systematic differences in textures and to qualitative classification schemes relating texture to the sample's thermal history (Champness and Lorimer, 1976; Lally *et al.*, 1975).

The purpose of this paper is to provide a calibration of the relation of submicroscopic exsolution textures in augite rims of lunar pyroxene-porphyritic basalts to the sample's thermal history. Pyroxene exsolution textures have drawn the attention of optical petrographers (Hess, 1960; Robinson *et al.*, 1971, 1977) who described them in the Stillwater, Skaergaard and Bushveld intrusions and predicted their usefulness as recorders of cooling rate. For this study the Apollo 15 quartz-normative basalts were chosen. The Apollo 15 QNB suite is comprised of pyroxene-porphyritic samples that cooled in a lava flow or shallow intrusive. The hand specimens vary from vitrophyres to microgabbros and sample a cooling unit on the order of 10 meters or greater in thickness (Grove and Walker, 1977). These samples show dramatic intragroup variations in texture, but little variability in the bulk composi-

0003–004X/82/0304–0251$02.00

tion, and represent a magma body that experienced a wide range of cooling histories, but was not affected by differentiation. Bence and Papike (1972) described the complex chemical zoning in pyroxenes from these samples and used these variations to infer crystallization histories and relative cooling rates. Experimental investigations (Lofgren *et al.*, 1974; Grove and Bence, 1977) reproduced the compositional variations in pyroxene phenocrysts and the accompanying textural differences through cooling rate experiments. Thus, the Apollo 15 QNBs are well characterized and provide excellent starting materials for a detailed study of the response of submicroscopic pyroxene exsolution textures to variations in thermal history. A series of cooling rate experiments (Grove and Bence, 1977) on Apollo 15 quartz-normative basalts (QNBs) produced pyroxenes with known thermal histories. Observations of these synthetic samples and of clinopyroxenes from Apollo 15 QNB collection (15597, 15499, 15058) are used to infer exsolution mechanisms and to calibrate the relation of coarsening rate to cooling history.

Pyroxene compositional variation: relation to temperature and cooling history

In a previous study (Grove and Bence, 1977), linear cooling rate experiments were designed to examine the effects of variable cooling rate on phase appearance temperatures, phase compositional zoning and liquid line of descent in the QNBs. The experiments were initiated at a ~10°C superheat, cooled at a chosen linear rate to a desired temperature and quenched into water to terminate the experiment. The experiments chosen for the TEM study (Fig. 1) are plotted along with curves which illustrate the effect of variable cooling rate on phase appearance temperature. Pigeonite (Wo_5En_{68}) is a near liquidus phase and forms the cores of phenocrysts. As crystallization continues the pigeonite becomes increasingly iron and calcium rich, until an augite rim forms on the pigeonite phenocryst core. The rim crystallizes as a consequence of the suppression of plagioclase nucleation and growth, which causes the residual liquid to become enriched in Ca (Grove and Raudsepp, 1977). As cooling rate decreases, development of augite rims is not as pronounced. This effect can be seen by comparing the pyroxene zoning trends produced in progressively slower cooling rate experiments and in slowly cooled lunar microgabbro 15058 (Fig. 2).

At a cooling rate of 150°C/hr a Ca-rich rim grows over a long temperature interval, (Fig. 2a), and the rim also incorporates large quantities of Al and Ti. Plagioclase fails to appear under these conditions. At a 0.5°C/hr cooling rate the augite rim (Wo_{30-35} En_{40-35}) forms at 1100° and grows until the appearance of plagioclase at 1040°C causes a low-Ca clinopyroxene or augite + pigeonite assemblage to form as groundmass (Fig. 2b). Several lunar samples experienced slow cooling, which is evidenced by their textural characteristics and in their pyroxene zoning trends (*e.g.*, 15058). Under these conditions pyroxene phenocrysts are still texturally evident, but the Ca-enrichment in the rim is less pronounced (Fig. 2c), and the groundmass two-pyroxene + plagioclase intergrowth is less distinctive than in the more rapidly-cooled porphyritic samples.

The augite rim appears at ~1100°C over the range of cooling rates experimentally studied (Fig. 2), is a texturally and chemically distinctive marker in the crystallization history of the clinopyroxene phenocrysts, and as such provides a known starting point for calibrating a QNB's cooling history. TEM observations made on the lunar and synthetic samples located this composition zone in the clinopyroxene, and it is assumed that the recorded thermal histories were initiated at or shortly after this initial temperature.

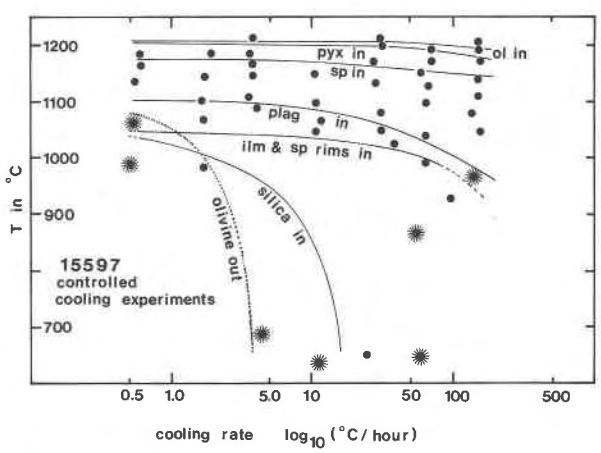

Fig. 1. Cooling rate experiments on lunar quartz-normative basalt 15597. Experiments were initiated at 1225±5°C, cooled at the desired rate to a temperature indicated by the dot or star and terminated by quenching into water. Lines show the temperature below which a phase appears or disappears. The augite rim grows at 1100°C for all cooling rates. Stars represent experiments selected for TEM analysis (see Table 1).

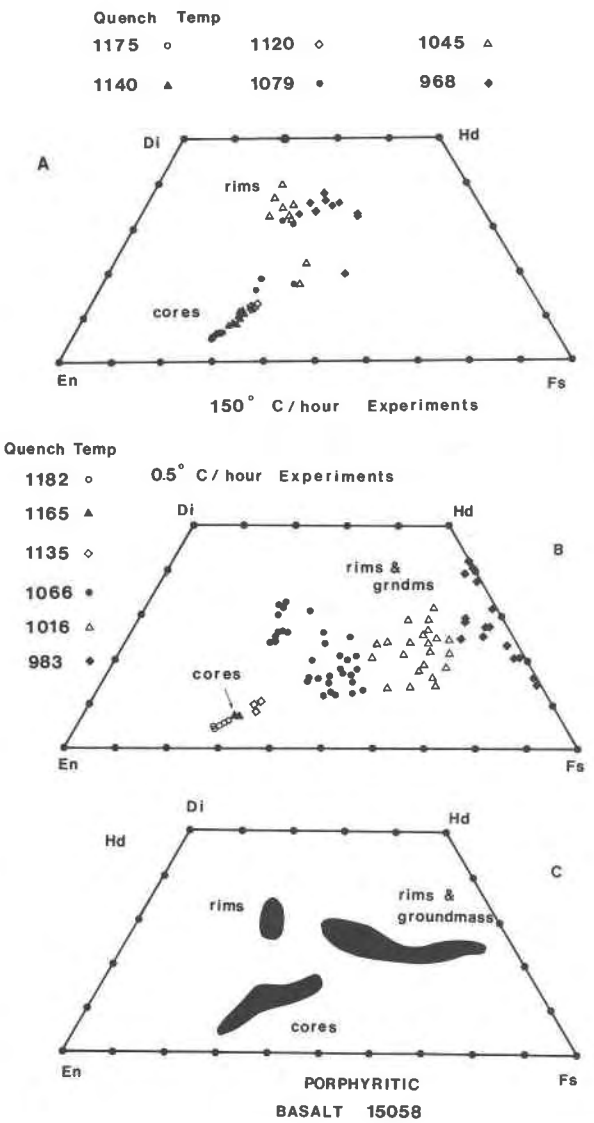

Fig. 2. (a) Ca–Mg–Fe compositional zoning trend. Pyroxenes from 150°C/hr experiments. This zoning trend is compiled from analyses of pyroxene phenocrysts in all 150°C/hr experiments. To avoid overlapping zoning profiles only the portion of the trend produced in the temperature interval between quenched runs is shown. Thus each symbol represents the compositional variation produced between the quench temperature of the previous run and the quench temperature indicated by the symbol. Note that the augite rim has formed in the temperature interval 1120° to 1079°C. (b) Pyroxene Ca–Mg–Fe zoning trends in 0.5°C/hr experiments. (c) Ca–Mg–Fe zoning trends in 15058 (taken from Bence and Papike, 1972).

Experimental

Clinopyroxene phenocrysts produced in linear cooling rate experiments (Grove and Bence, 1977) and lunar pyroxenes (15597,64, 15499,98 and 15058,99) were selected for TEM examination. The experiments span cooling rates of 0.21°C/hr to 150°C/hr and the run conditions of experiments observed with the TEM are plotted in Figure 1 and summarized in Table 1.

Standard petrographic thin sections polished on one side were prepared using thermally-sensitive cements (Lakeside or Crystalbond) and areas were selected for TEM examination. The thin sections were removed from their glass slides and selected portions were mounted between 3 mm diameter Cu grids with epoxy. Areas of interest on the grid were analyzed with the electron microprobe to infer the bulk composition, and samples were thinned using an ion micro-milling device.

Observations were made with a Philips EM300 microscope operating at 100 kV. A VGHB5 scanning transmission electron microscope (STEM) was used to obtain quantitative analyses of regions in which lamellae width measurements were made. Magnification was obtained periodically by using a grating replica standard. With the exception of #95, #116 and lunar sample 15058, each lamellar wavelength reported in Table 2 is the mean from all traverses made on a single micrograph. Several traverses were made on each micrograph, the number of lamellae for each traverse was counted, a wavelength was obtained, and wavelengths from each traverse were averaged. The variability in lamellae periodicity is well represented by the variability in the measurements listed in Table 2, and in general the standard deviation increases as lamellae wavelength increases. For a typical traverse made in the 3.6°C/hr pyroxenes the mean wavelength was 222 ± 28Å. For experiment #95, #116 and lunar sample

Table 1. Run conditions of cooling rate experiments selected for TEM study

Rate °C/hr	Run#	Duration+	T_{init}	T_{fin}
150	63	1.7	1223	968
60	32	9.6	1224	649
63	34	3.8	1227	992
11	39	52.2	1221	632
3.6	48	148.8	1220	689
0.56	75	280.6	1223	1066
0.50	95	481.6	1226	983
0.21	116	1771.1	1217	845

+*Experiments were held at the indicated initial temperature for 0.5 hours and then cooled at the specified rate for the indicated times (hours). The experiment was terminated by quenching into water. Temperatures are in °C.*

Table 2. Lamellar wavelengths measured in pyroxenes from cooling rate experiments and lunar samples

		Spinodal*		Homogeneous		Heterogeneous		Δβ
		(001)	(100)	(001)	(100)	(001)	(100)	
Experiments								
Run #	Cooling rate °C/hr							
63	150	90	86			630	none	0.81
32	60	130,160,141	104,80,113			820,535,570	none	2.32
34	63	159,135	125,102			915	none	
39	11	203,178	142			present	none	2.9
48	3.6	222,207,210, 196,233,255 *mean=221*	176,202			1490,1585,2041	present	2.93
75	0.56	240,243,233, 238,237,257, 202 *mean=236*	present	820,863, 995		2105,1396	1580,1079	
95	0.5	247,290,284, 381,216,255, 242,353,237, 282,282,323, 346,290,266, 282 *mean=286*	232	625,616, 524	825,701, 897,525, 656,627, 715	2105,1396,2326 2167,1984,1903	1580,1079, 1220,1300, 1476	2.93
116	0.21	431,311,399, 417,440,773, 692,691,394, 395,403,376, 389,468 *mean=469*	present	922,883, 1165,900, 914,935	1272	present	1825,2924, 2698,2118	
Lunar Samples								
Sample #								
15597,64		165,170	present			576	none	
15499,98		186,176,196 *mean=186*	present			present	none	2.67
15058,99		919,1289, 616,730, 1178,1256, 602,1373 *mean=995*	702			present	4578,5695, 3854,2698	2.86

*Wavelengths are cited in Angstrom units. Each number represents measurement of lamellae on a separate micrograph.

15058 the average wavelength for each traverse is listed. Wavelengths are variable and bimodal in these slowly-cooled clinopyroxenes. Regions that contained homogeneously-distributed exsolution lamellae with volume proportions of augite and pigeonite near 50–50 or 40–60 were chosen for measurement. If one phase predominated (*e.g.*, 10% augite and 90% pigeonite), the region was excluded from the wavelength data set.

TEM observations of microstructures in experimentally-produced clinopyroxenes

Augite rims in 150°C/hr and 60°C/hr cooling rate experiments exhibit fine (001) and (100) exsolution lamellae (Fig. 3a, b) with a "tweed" texture. Larger "tongue and groove" lamellae on (001) (Fig. 4) are present at the interface between the augite rim and pigeonite core. The tweed exsolution may be best observed using a $C2/c$ reflection and has a wavelength on the order of 90Å at 150°C/hr and 135Å for the (001) and 110Å for the (100) orientation in 60°C/hr experiments (Table 2). The larger "tongue and groove" lamellae are pigeonite which contain small 100Å-scale APD's (antiphase domains) that nucleated as a consequence of the $C2/c \rightarrow P2_1/c$ phase transition (Fig. 4b). Images of the tweed region do not show discreet pigeonite lamellae with a $P2_1/c$ structure. The larger set of (001) lamellae are always associated with solitary dislocations or a line of dislocations in a subgrain boundary (Fig. 4a). It appears that these larger lamellae have used the preexisting defects as sites for heterogeneous nucleation. Similar textural relations are found in the augite rims of 10°C/hour experiments.

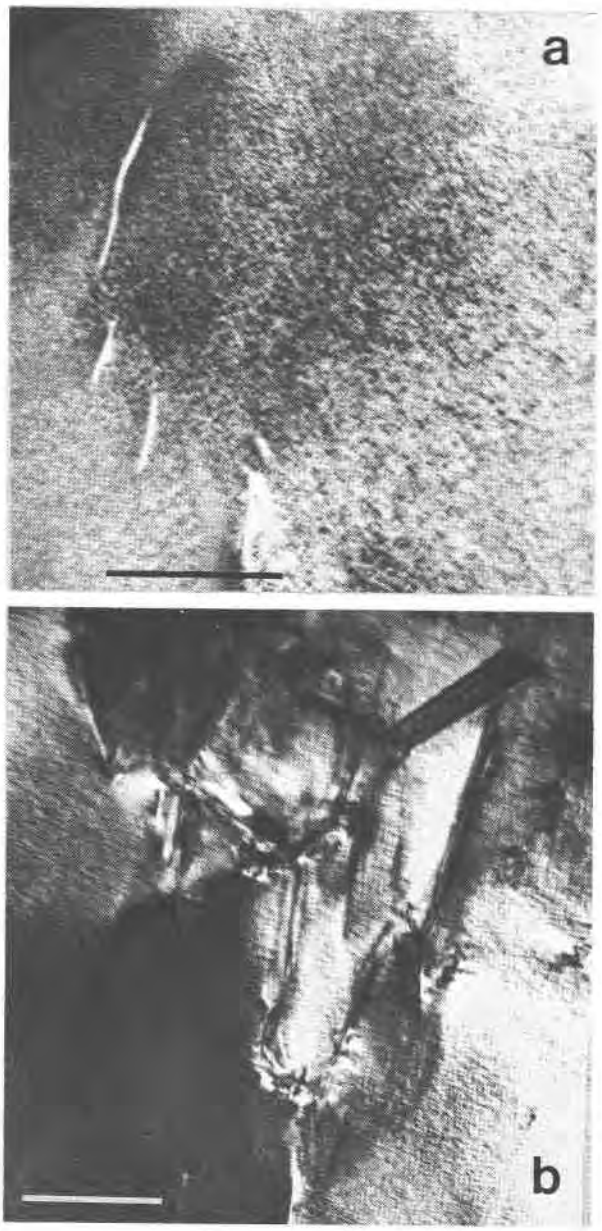

Fig. 3. (a) Tweed texture in pyroxene from 150°C/hr cooling rate experiments. (597-63). DF (dark field), g = 002 (b) Tweed texture in pyroxene produced in 60°C/hr experiment (597-32). DF, g (reciprocal lattice vector) = 202. Scale bars are 0.5 microns long.

Diffraction patterns taken in the augite rim regions of 60°C/hr tweed show weak diffuse h + k odd spots (characteristic of $P2_1/c$) and strong h + k even spots (characteristic of $C2/c$) that are streaked parallel to both a^* and c^* (Fig. 5a). It is not possible in these augite rims to resolve discreet diffraction maxima corresponding to the coexisting augite and pigeonite. In contrast, h + k odd pigeonite reflections are sharper in 10°C/hr augite rims and in addition two h + k even maxima are evident. These maxima correspond to augite and pigeonite lamellae oriented nearly parallel to (001), and they are always connected by a streak indicating the existence of compositional range between the augite and pigeonite phases and suggestive of complete coherency between the two phases. Using the $\Delta\beta$ compositional estimation of Papike *et al.* (1971), the $\Delta\beta$ of $0.8\pm0.2°$ in 150°C/hr augite rims is consistent with a compositional difference of ~15 mole % Wo. Because there is compositional strain associated with the coherent lamellae, the betas for the intergrown phases will not have the same values as unconstrained augite and pigeonite, whose values are used to establish the $\Delta\beta$ relation. Thus, there is an unknown error in the $\Delta\beta$ technique, which involves

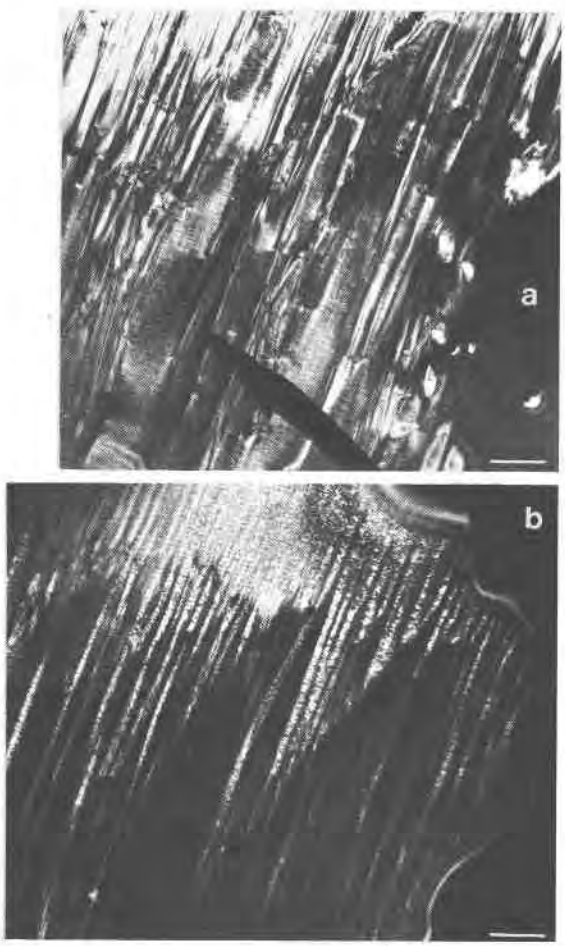

Fig. 4. Tongue and groove exsolution texture in 60°C/hr pyroxene (597-34). (a) The tweed texture is present in augite regions, and pigeonite lamellae have nucleated on defects. DF, g = 002. (b) Same region with a $P2_1/c$ reflection. DF, g = 102. Scale bars are 0.5 microns long.

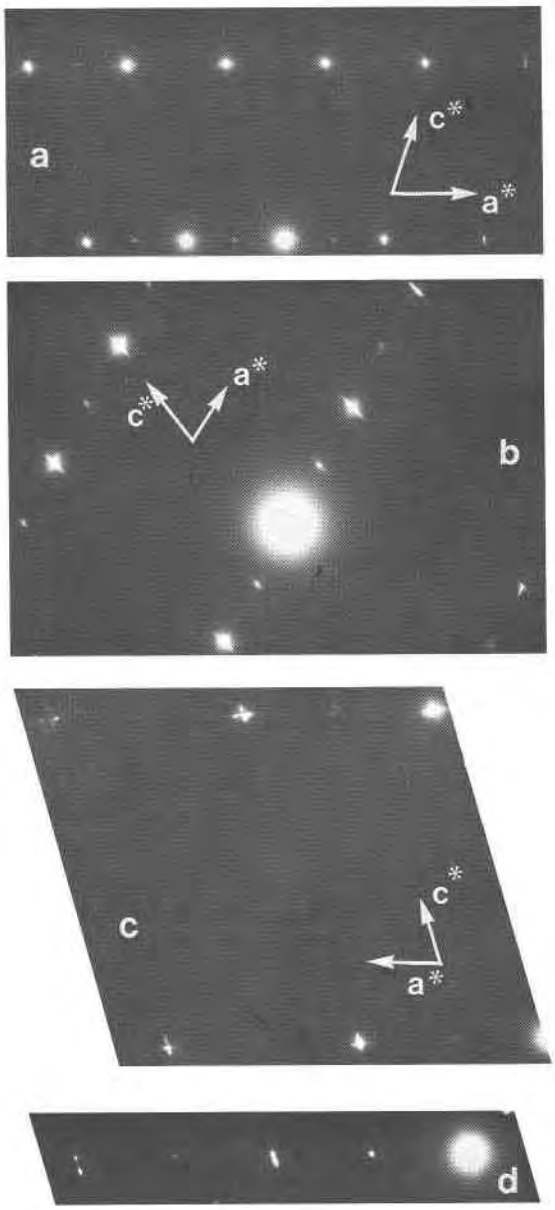

Fig. 5. Selected area diffraction patterns of the a^*–c^* net. a^* is the short reciprocal lattice direction and contains alternating $C2/c$ and $P2_1/c$ reflections. (a) 60°C/hr pyroxene. Spots are streaked perpendicular to (001) and (100). (b) 3.6°C/hr pyroxene (Fig. 6a). Two diffraction maxima are resolvable, one for pigeonite and one for augite (upper right), and streaks are perpendicular to (001) and (100). (c) Diffraction pattern from 0.5°C/hr pyroxene (Fig. 7a). Fine structure in diffraction spots results from multiple orientations of exsolution lamellae. (d) Spots from a region of 15058 containing homogeneous (001) lamellae. Streak indicates that lamellae are coherent.

a correction for strain. In the 60°C/hr augites, $\Delta\beta$ increases to 2.3±0.2° and indicates ~30% difference of wollastonite content. Lamellae in these rapid cooling rate experiments are too fine to analyze using the STEM, and therefore micro-analytical confirmation of lamellae compositions are not available.

The lamellae in the more slowly cooled experiments become progressively coarser (Table 2). Augite rims in 4°C/hr experiments contain (001) and (100) lamellae produced by a homogeneous mechanism (possibly spinodal decomposition) (Fig. 6) and heterogeneously nucleated lamellae approximately parallel to the (001) and (100) orientations. The diffraction spots for (001) pigeonite and augite (Fig.

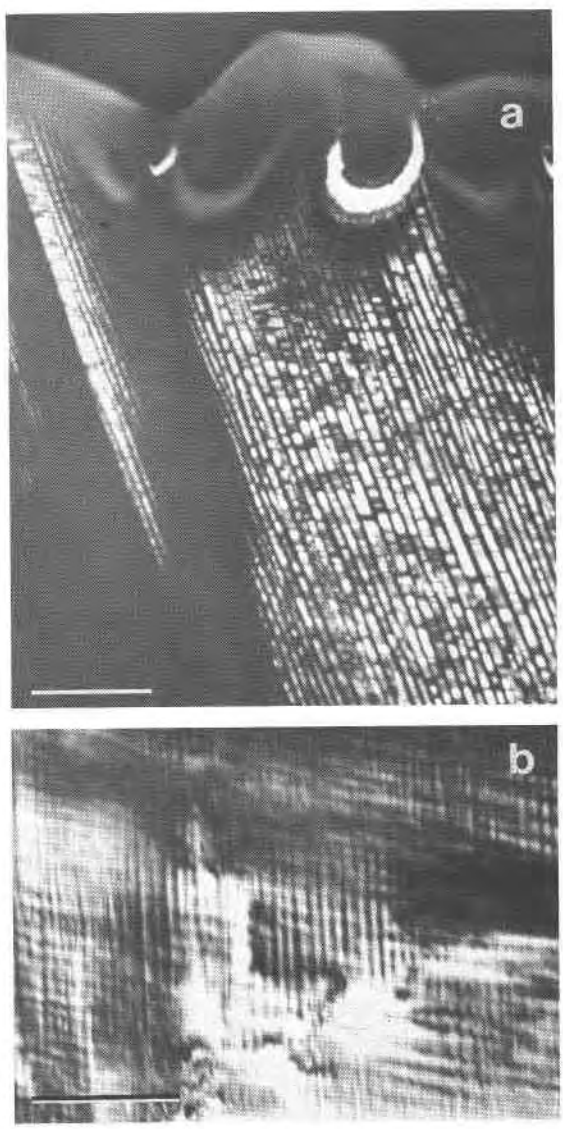

Fig. 6. Pigeonite-augite (001) lamellae in 3.6°C/hr pyroxene (597-48). (a) Distinctive regions of pigeonite are in contrast and contain APDs (antiphase domains) by the $C2/c$ to $P2_1/c$ transition. Areas of augite are out of contrast. DF, g = 102. (b) Tweed texture, g = 002. Scale bars are 0.25 microns long.

5b) now show two maxima, one for pigeonite and one for augite. In addition, streaking reveals the presence of lamellae perpendicular to the (100) orientation. In the 4°C/hr experiments, $\Delta\beta$ is $\sim 2.9 \pm 0.3°$, similar to the value measured in the 10°C/hr experiments. In the homogeneously-produced exsolution lamellae, there are distinct regions of $P2_1/c$ pigeonite. When observed in dark field using a h + k odd reflection, the pigeonite regions contain oriented antiphase boundaries and show sharp boundaries with the enclosing augite (Fig. 6a).

Exsolution textures in the augite rims of 0.5°C/hr and 0.21°C/hr cooling rate experiments contain different microstructures characteristic of slower cooling rates. Larger, distinctive heterogenously-nucleated (001) and (100) lamellae are present, which in turn, contain a finer set of heterogeneously-nucleated lamellae (Fig. 7a).

In heterogeneously-nucleated (100) lamellae the fine set is approximately parallel to (001). In the (001) heterogeneous lamellae the finer set is oriented near (001) (Fig. 7c), and sometimes (100) fine scale lamellae are present (Fig. 7a). The dominant submicroscopic textural elements observable in the augite rims are (001) lamellae produced by a homogeneous mechanism (Figs 7b, 7c, 8). Rarer (100) lamellae are also visible in dark field micrographs, taken using h + k even reflections. A tweed texture, which contains both (001) and (100) components (Figs. 7b, 8b) is also present. Generally, only the (001) set of tweed shows the contrast characteristic of pigeonite that has transformed to $P2_1/c$ when an h + k odd spot is used to form a dark field image, but a rare pigeonite lamellae in the (100) orientation may be found (Fig. 8a). Apparently, the (100) set of lamellae, though present in the augite, has not decomposed to compositions that will transform to $P2_1/c$ structure on cooling.

Similar textural relations are present in the augites of all 0.5°C/hr and 0.2°C/hr cooling rate experiments. The augite rim of an experiment quenched at 1066°C, 44°C below the nucleation temperature of the augite rim, shows both (001) and (100) orientations produced by coarsening of spinodally-produced lamellae (Fig. 8b). In pyroxenes quenched in lower temperature 0.5°C/hr and 0.2°C/hr cooling rate experiments an additional lamellar morphology is present. A set of (001) and (100) lamellae with longer wavelength, similar to the homogeneous morphologies found in pyroxenes from other cooling rate experiments, is rarely observed (Fig. 7a). Diffraction patterns from regions of intergrown spinodally-produced, homogeneously-nucleated and heterogeneously-nucleated (001) and (100) lamellae are complex (Fig. 5c). Streaks are present on both $C2/c$ and $P2_1/c$ reflections, indicating the presence of compositional fluctuations within both the coarse set and the finer set of (100) and (001) orientations. Separate diffraction maxima are associated with the heterogeneously-nucleated (100) and (001) orientations of pigeonite and augite. In a region containing pigeonite/augite intergrowths produced by spinodal decomposition, diffraction pattern morphology is simple (Fig. 5d). Here, the pigeonite/augite spots are distinct with $\Delta\beta \sim 2.9°$ and are connected by a streak indicating the existence of a compositional fluctuation between the two phases.

The lamellar morphology observed in 0.2°C/hr experiments is similar to that of the 0.5°C/hr pyroxenes. The compositions of lamellae in a 0.2°C/hr pyroxene were obtained with the STEM in regions containing lamellae texturally similar to Figure 7a and 7c. The volume proportions of pigeonite and augite range from being nearly equal to 10%–90%. However, the compositions of the coexisting lamellae were found to be independent of the volume proportions, indicating that submicroscopic compositional differences that can be seen in Figure 7a and 7c are the result of variations in Ca content produced during growth from the melt. A consequence of this submicroscopic compositional variation may be seen in microprobe analyses of the augite rims (Fig. 2), which commonly show a spread in Ca content and a constancy in Fe/Mg ratio. Regions of lamellae produced by spinodal decomposition and coarsening have a wavelength of 450Å and are $Wo_{35}En_{37}$ and $Wo_{12}En_{42}$, a compositional separation in %Wo consistent with that obtained from the $\Delta\beta$ spread. The STEM analyses were calculated using the k ratio technique of Cliff and Lorimer (1975) and a pigeonite Wo_5En_{68}, an augite $Wo_{47}En_{48}$ and a hedenbergite $Wo_{49}En_{18}$ as standards. Errors in replicate analyses made during different STEM sessions were ±2% Wo and ±2% En.

TEM observations of microstructures in lunar samples

The lunar samples 15597, 15499 and 15058 were chosen for TEM study. In 15597, (Table 2) the fine scale tweed (001) and (100) modulation was observed. In 15499, tweed modulation and heterogeneously-nucleated (001) lamellae were observed

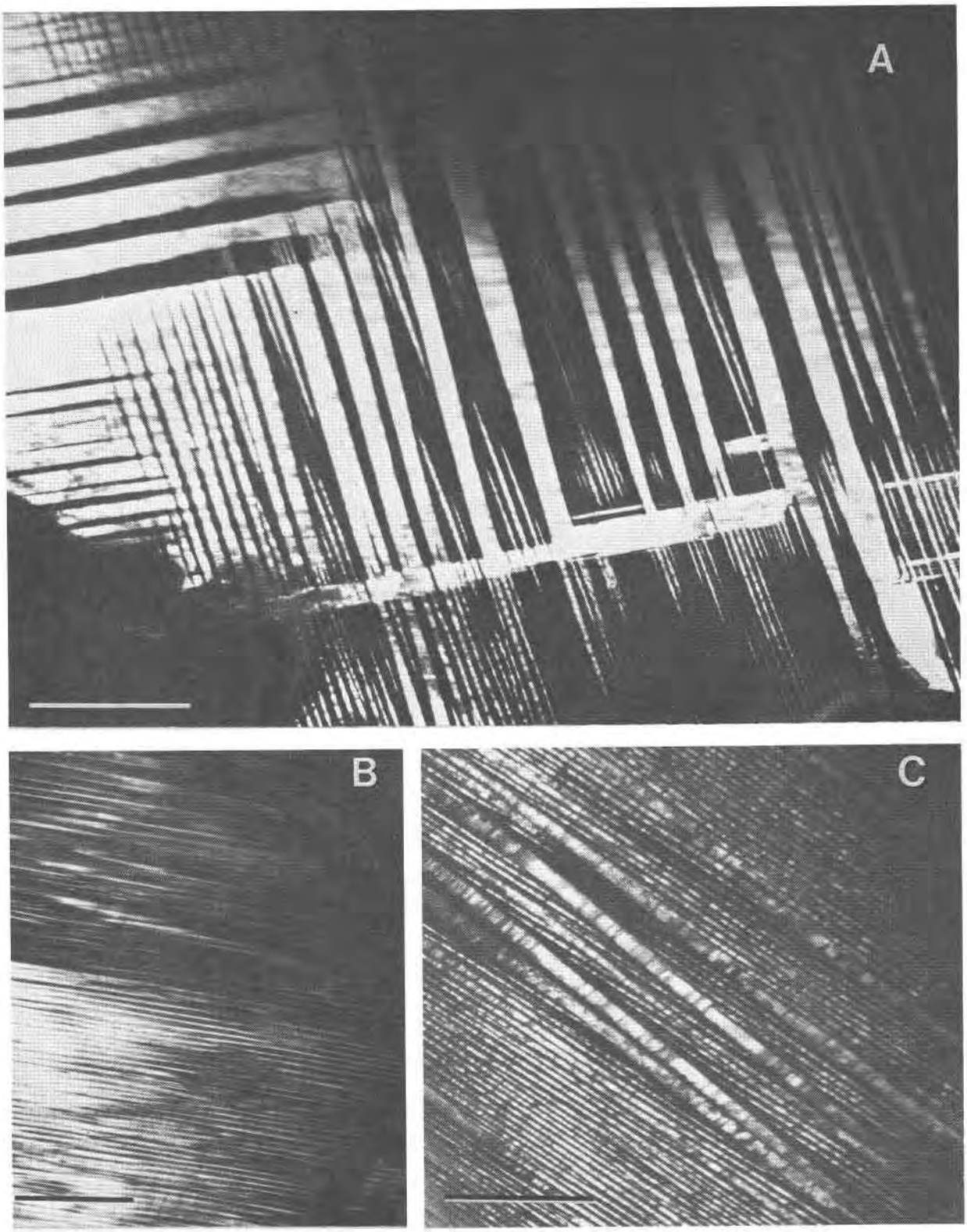

Fig. 7. Exsolution textures in pyroxenes from 0.5°C/hr experiment (597-95). (a) Multiple orientations of exsolution lamellae observed with an $h + k$ odd reflection. Light areas are pigeonite and contain domains resulting from $C2/c$ to $P2_1/c$ transition. Augite regions are dark. DF, g = $10\bar{4}$. (b) Region near (a) taken using a $C2/c$ reflection. Tweed contrast from (100) lamellae parallels NE-SW. DF, g = 202. (c) Heterogeneously-nucleated (001) lamellae surrounded by homogeneously nucleated (001). DF, g = 102. Scale bars are 0.5 microns long.

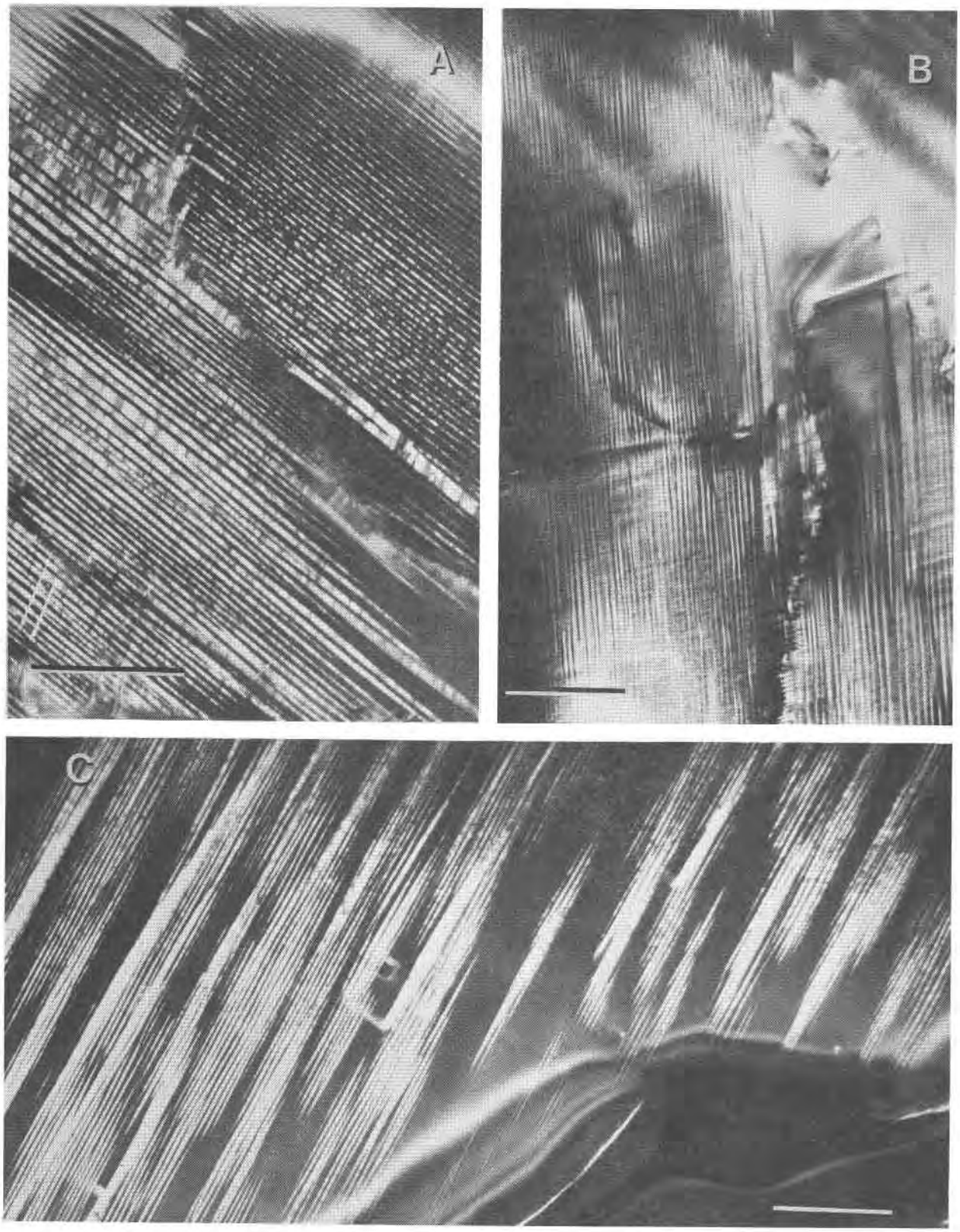

Fig. 8. Exsolution lamellae in pyroxenes from 0.5°C/hr experiment (597-75). (a) Region of homogeneously and heterogeneously-nucleated (001) lamellae. The boundaries of the two lamellae are rotated by several degrees. DF, g = $40\bar{5}$. (b) Both (001) (E–W) and ($10\bar{0}$) (N–S) homogeneously-nucleated lamellae are visible. Boundary between augite rim and pigeonite core is in upper right. DF, g = $40\bar{4}$. (c) Homogeneous (001) lamellae with $\lambda = 232$Å show a long period modulation. DF, g = $40\bar{5}$. Scale bars are 0.5 microns long.

(Fig. 9a). Streaking of diffraction maxima is found in regions of tweed exsolution texture (Fig. 9b).

Sample 15058 contains microstructures similar to those developed in pyroxenes of slow cooling rate experiments. Large regions of augite contain coherent (001), rare (100) lamellae (Fig. 10b,d), and a bimodality in the thickness of intergrown pigeonite/augite lamellae is often evident. Heterogeneously-nucleated lamellae contain finer coherent lamellae. In Figure 10a,c large (100) lamellae are filled with a finer-scale intergrowth of (001) pigeonite and augite.

Augite compositional variation in 15058 is greater than in the rims of slowly-cooled experiments. STEM analyses of the region shown in Figure 10a are $Wo_{11}En_{30}$ and $Wo_{35}En_{26}$, whereas the regions of Figure 10b,d are $Wo_{12}En_{37}$ and $Wo_{35}En_{35}$.

Interpretations of microstructures

The exsolution morphologies observed in the experimentally produced and lunar pyroxenes formed by two separate homogeneous exsolution mechanisms and by heterogeneous nucleation. The large heterogeneously distributed lamellae have nucleated on preexisting dislocations or subgrain boundaries (Figs. 4,7a,8a). These lamellae which nucleated heterogeneously have been observed in other lunar and terrestrial clinopyroxenes (Champness and Lorimer, 1976; Nord *et al.*, 1976).

The second prominent lamellar morphology is the tweed texture observed in rapidly-cooled augites (Figs. 3,4a) which coarsens into a regular coherent exsolution texture at slower cooling rates (Fig. 6). This morphology was observed in lunar and terrestrial pyroxenes (Champness and Lorimer, 1976; McCallister, 1980) and in isothermally-annealed synthetic clinopyroxenes (McCallister, 1978; Buseck *et al.*, 1980). The following textural aspects of these lamellae suggest that they formed by spinodal decomposition (Cahn, 1968). If spinodal decomposition were the mechanism of formation, one would expect a continual change in the compositions of coexisting lamellae to occur during the decomposition process. At the beginning of spinodal decomposition the compositional differences increase, until finally two compositionally distinct lamellae are present (see Fig. 3, Nord *et al.*, 1976). Evidence for this process is found in diffraction patterns of the tweed exsolution texture. In pyroxenes cooled at 150°C/hr and 60°C/hr, diffraction patterns contain only one reciprocal lattice. The diffraction spots show streaking parallel to a^* and c^*, but the angular difference between the augite and pigeonite spots is small. This is consistent with a small difference in composition between the coexisting lamellae. As cooling rate decreases, the compositional difference, estimated using $\Delta\beta$, increases continually (Table 2). At rates slower than 10°C/hr, spinodal decomposition is complete and coarsening of the lamellae continues.

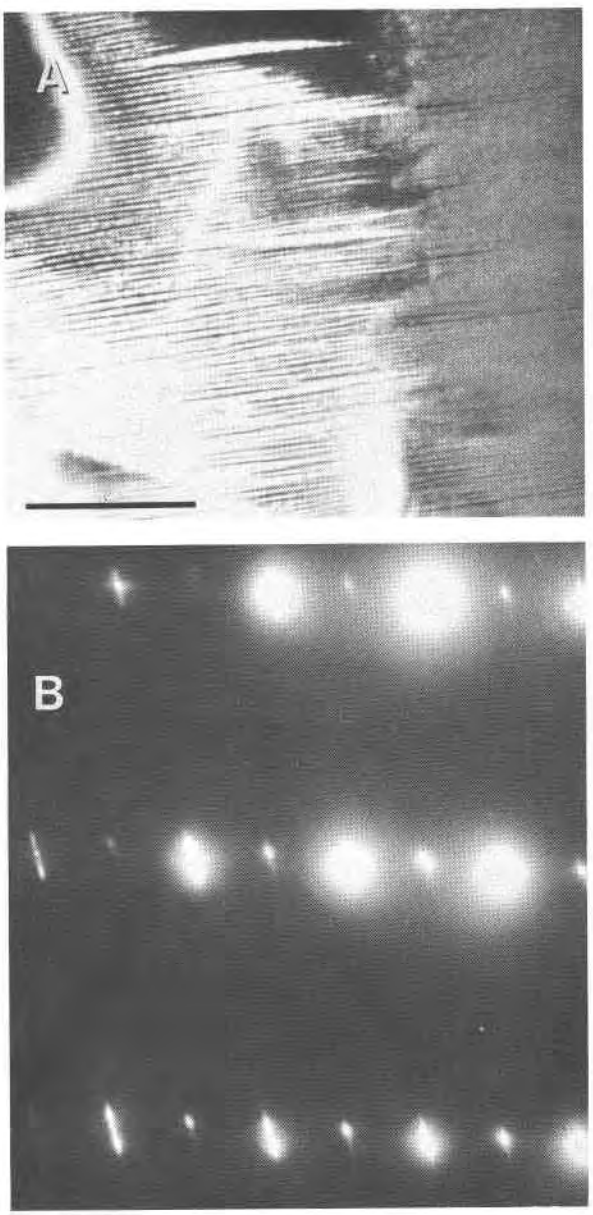

Fig. 9. (a) 15499 augite rim containing (001) lamellae produced by spinodal decomposition and coarsening. DF, g = $40\bar{3}$. Scale bar is 0.5 microns long. (b) Selected area diffraction pattern of (010) pole a* is horizontal. Streaks are perpendicular to (001) and (100) lamellar orientations.

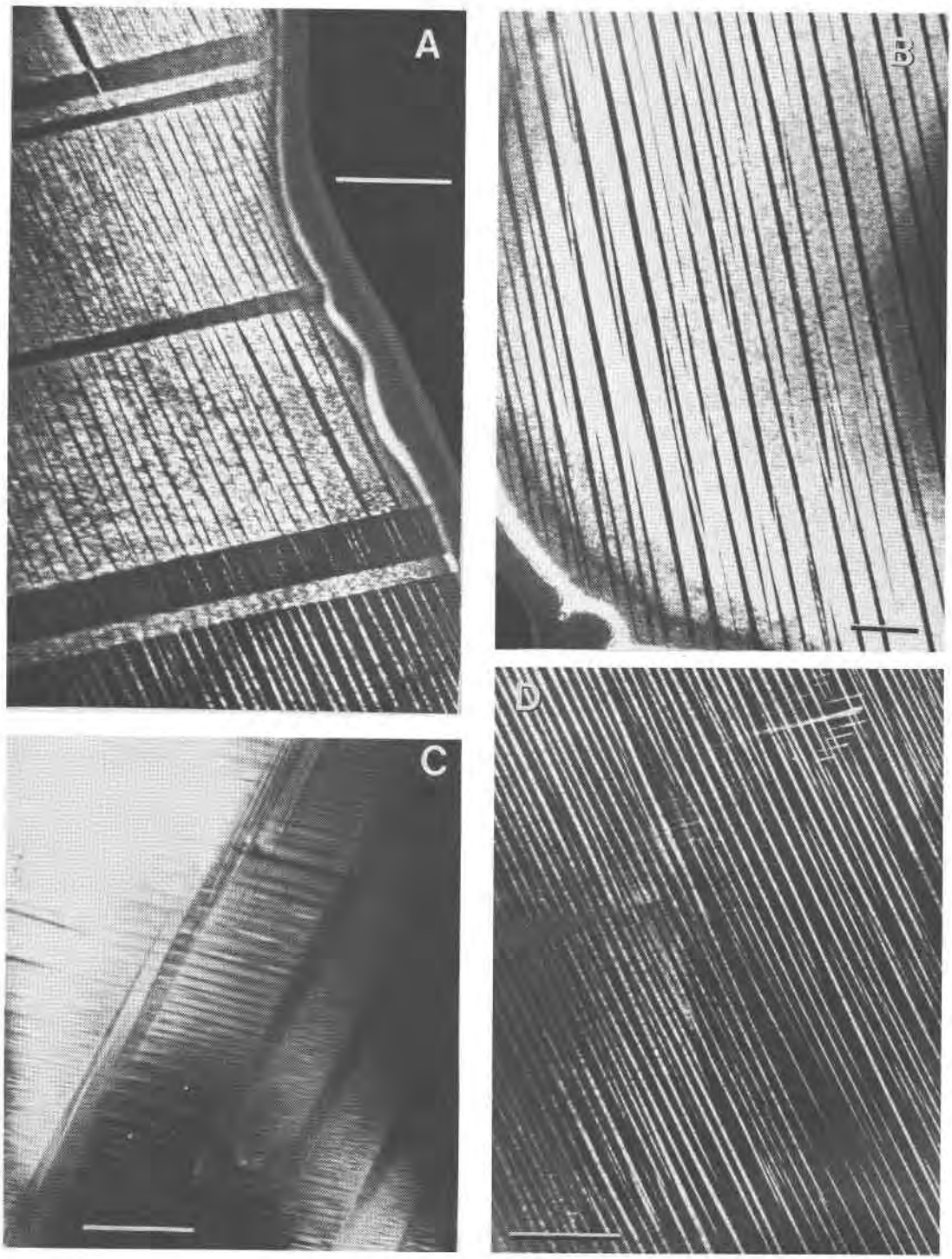

Fig. 10. Exsolution textures in pyroxenes from lunar sample 15058. (a) Multiple orientations of lamellae are evident. Heterogeneous (100) lamellae contain finer scale homogeneous (001) lamellae. DF, g = $10\bar{2}$. (b) Homogeneously-nucleated (001) lamellae in pigeonite have coarsened by selective removal of interspaced augite lamellae. The tips of lamellae moving to subgrain boundaries in opposite directions have become pinned. DF, g = $10\bar{2}$. (c) Contrast from a region near (a) obtained with a *C*2/*c* reflection shows the persistence of the homogeneous (100) orientation. DF, g = 002. (d) Homogeneous (001) lamellae in augite. The rare (100) orientation is visible in upper right. DF, g = $10\bar{2}$. Scale bars are 0.5 microns long.

The fine tweed texture consists of two orientations, one near (001) and the other near (100). Through the spinodal mechanism the preferred orientation for amplification will be one that minimizes coherency strain energy and that has the maximum diffusion rate. Both (001) and (100) result in a lower elastic strain energy, but the (001) orientation gives the lowest strain energy (Morimoto and Tokonami, 1969; Tullis and Yund, 1979). Because both orientations are observed, their spinodals are at equal temperatures, suggesting that the rate-controlling factor causing the (001) lamellae to be the preferred amplification orientation is diffusion. Diffusion is faster perpendicular to (001) and these lamellae are the preferred set. It is notable, however, that the (100) orientation is persistently present in all pyroxenes, in the most rapidly cooled sample (Fig. 3), in the slow cooling rate experiments (Figs. 7b,8b) and in the most slowly cooled lunar sample (Fig. 10c). Only rarely does this orientation coarsen to compositionally distinguishable $P2_1/c$ pigeonite and $C2/c$ augite (Fig. 10d). In most samples, it retains a small compositional fluctuation, evidenced by the weak diffraction contrast and streaking of diffraction patterns (Fig. 5).

The effect of continuous cooling on the lamellae of the (001) orientation is continual increase in spacing as cooling rate decreases. This increase suggests that the formation temperature of 1100°C for the augite rim is well below the critical temperature for the coherent spinodal. Cahn (1968) provided a formulation for the variation in the initial lamellae wavelength (λ_0) *vs.* undercooling for isothermal spinodal decomposition. The value of λ_0 changes from infinity to a few hundred Ångstroms at 1° undercooling and over the next 100° changes less than an order of magnitude. Huston *et al.* (1966) discussed the change in λ_0 with cooling rate, and showed that λ_0 decreases as the 1/6 power of cooling rate, if complete decomposition occurs. If it is assumed that the three rapid cooling rate experiments record the rate dependence for λ_0 and that the lamellae have completely decomposed, and have not begun to coarsen, the exponent for the effect of rate on λ_0 is 1/4.

Observations of larger (001) and (100) lamellae in 0.5°C/hr and 0.2°C/hr cooling rate experiments suggest that lamellae nucleate homogeneously only rarely under these slower cooling conditions. Nord *et al.* (1976) also inferred the existence of homogeneously-nucleated lamellae in 70017 augites (Table 2).

A striking feature of some regions containing lamellae is the presence of a longer wavelength modulation superimposed on the finer scale spinodal modulation (Figs. 6a,8c). The formation of multiple wavelengths may occur during the spinodal decomposition process. Cahn (1968) calculates the wavelength having the maximum amplification rate, but he points out that other wavelengths may also grow at a slower rate in comparison to the fastest. The longer wavelength features (λ = 0.5–0.9 microns) present in the augite rims may form during the initial stages of decomposition, but are overtaken by coarsening on the wavelength for most rapid growth; the abundant (001) modulation with λ of several hundreds of Ångstroms. Alternatively, Figure 8c may be an area of original tongue and groove which has undergone spinodal decomposition.

TTT diagram

A useful representation of the exsolution kinetics that allows one to show the exsolution mechanisms which operate for a particular thermal history is the TTT diagram (Time–Temperature–Transformation) (McConnell, 1975, Putnis and McConnell, 1980). A transformation (*e.g.*, exsolution) is represented as C-shaped start and finish curves on a log time *vs.* temperature plot. The start curve represents the beginning of the transformation and in the case of spinodal decomposition its shape is determined by the interrelation of decreasing diffusion rate and decreasing initial wavelength (*i.e.*, decreasing diffusion distance). For nucleation the shape is controlled by decreasing diffusion rate and increasing lamellae nucleation rate. The two different processes produce curves with similar shapes. The nose of the TTT curve occurs at a temperature and time for which diffusion rate is rapid and initial wavelength or nucleation rate is optimal for exsolution. Diffusion rate continually decreases with decreasing T, whereas nucleation rate or initial wavelength reaches a minimum near the critical temperature, increases to a maximum at a particular undercooling, and decreases again at larger undercoolings. The finish C-curve has a shape similar to the first, and indicates the termination of the exsolution transformation.

A set of TTT curves for the augite–pigeonite exsolution mechanisms is constructed in Figure 11. Heterogeneous nucleation involves a lower free energy barrier than homogeneous nucleation and takes place at small undercoolings. The composition of lamellae and host will be those of the

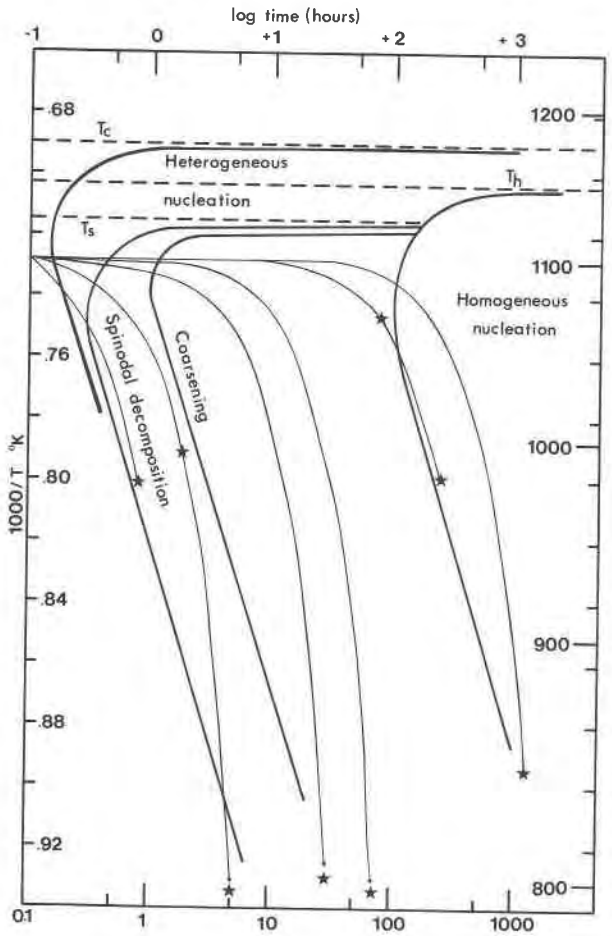

Fig. 11. TTT (Time–Temperature–Transformation) diagram for QNB augite rims constructed using TEM observations of experimental data. The light lines outline the cooling paths of linear rate experiments. Stars mark the termination temperature of the experiment. Dark curves are the C-shaped start curves for heterogeneous nucleation, spinodal decomposition, coarsening of spinodally-produced lamellae and homogeneous nucleation. Temperature for the critical point (T_c) is inferred from experiments by Ross *et al.*, 1973. Temperatures for the coherent solvus T_h and coherent spinodal T_s are inferred. Slopes of curves are estimated using the method described by Putnis and McConnell (1980).

equilibrium solvus. Thus, the curve for heterogeneous nucleation is placed directly below the inferred solvus temperature of 1175°C, determined by Ross *et al.* (1973) from heating experiments on clinopyroxenes from 12021, similar in composition to the rim augites of this study (Fig. 2). Decomposition by the spinodal mechanism will occur below the temperature of the coherent spinodal. The coarsening behavior of the lamellae indicates that this temperature is above 1100°C and it is estimated at 1125°C in Figure 12. This estimate is made assuming a temperature difference between the equilibrium solvus and the coherent spinodal similar to that predicted by Tullis and Yund (1979). The temperature for homogenous nucleation is estimated to be 15°C higher than the spinodal temperature. The exsolution temperatures will change, as can be inferred from Figure 12, by changes in the bulk composition of the clinopyroxene that is undergoing exsolution. The position of the start curve for homogenous nucleation is drawn to be consistent with the observations of textures in the slow cooling rate experiments.

Coarsening kinetics

After spinodal decomposition of exsolution lamellae has occurred, the lamellae coarsen according to a simple rate law. The rate law applies only to the coarsening of lamellae that have finished decomposing by the spinodal mechanism and that are

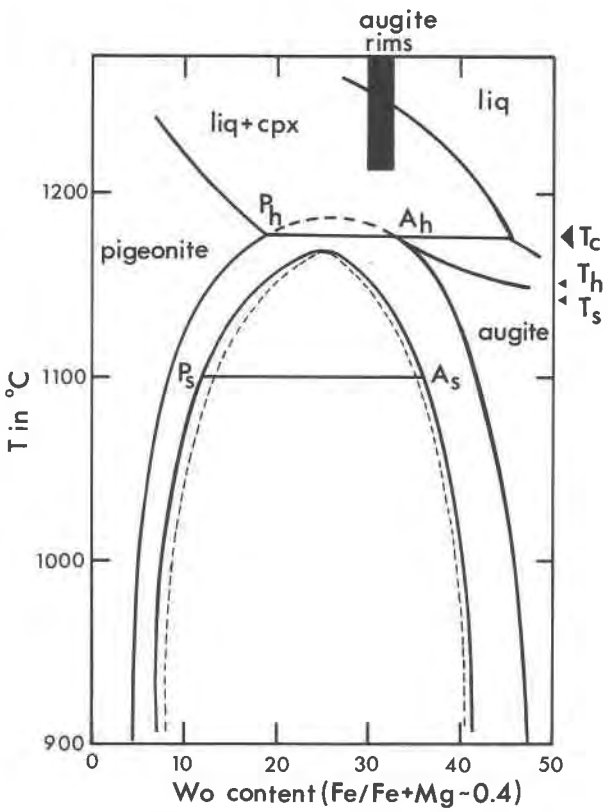

Fig. 12. Equilibrium phase diagram for a cross-section of the pyroxene quadrilateral at Fe/(Fe+Mg) = .40. Augite rims grow at 1100°C and undergo heterogeneous exsolution to compositions P_h-A_h. Spinodal decomposition within the coherent spinodal produces coexisting lamellae P_s-A_s.

in the process of coarsening by diffusion-controlled growth. The law is of the form:

$$\lambda = \lambda_0 + kt^{1/3}$$

where λ is lamellae wavelength, λ_0 is an initial wavelength, k is a rate constant and t is time. The coarsening kinetics of a synthetic clinopyroxene composition ($Wo_{27}En_{73}$) were found to follow a $t^{1/3}$ rate law for coarsening during isothermal annealling (McCallister, 1978). McCallister also estimated an activation energy for coarsening of 99 kcal/mol, which is consistent with Ca diffusion as the rate controlling mechanism. Nord (1980) measured coarsening kinetics for synthetic Ca-Mg-Fe clinopyroxene ($Wo_{25}En_{31}$), and interprets the decomposition process to require rather long isothermal annealling times (see Buseck *et al.*, 1980, Fig. 22). He found that coarsening begins only after 1000 hours at the optimal temperature for diffusion rate and diffusion distance.

In the case of pyroxenes grown in continuous cooling experiments or pyroxenes produced during the crystallization of cooling lava flows or small plutonic bodies, isothermal coarsening behavior of exsolution lamellae may not be directly applied to determine cooling rates. Dynamic coarsening kinetics will differ because continuously increasing the undercooling changes the coarsening rates of lamellae by decreasing the diffusion rate of the rate-limiting species. Thus, lamellar coarsening will occur over a specific temperature interval, below which coarsening will not occur because it is inhibited by the decreased mobility of the rate-controlling species. In constructing a relation between the coarsening rate and the lamellar spacing one must estimate the temperature interval over which most of the coarsening occurs. This estimate, in turn, provides a cooling-rate speedometer. If one knows the temperature over which a process (*e.g.*, coarsening) takes place, and has an experimentally determined expression for the time required to produce the observed lamellar spacing, an average cooling rate may be obtained.

McCallister (1978) provided information on the temperature dependence of the rate constant for coarsening (see Fig. 3, McCallister, 1978). McCallister's rate constant and the coarsening rate integrated over the temperature interval 1100°C to 1066°C at 0.5°C/hr may be used to calibrate the dependency of coarsening in the Apollo 15 QNB pyroxenes. It is assumed that the slope of coarsening rate with temperature is similar to that determined by McCallister. This is a reasonable assumption, because it equates the activation energy barriers for both exsolution processes. The modified temperature dependency of the rate constant is:

$$\ln k = -17.3 \times \frac{1000}{T} + 17.2 \qquad (T \text{ in K})$$

Integration of this rate constant over temperature predicts that >90% of the coarsening will have occurred over the interval 1100° to 900°C, and 98% over the interval 1100° to 800°C. Thus, the spinodally-produced lamellae in augite rims provide a cooling rate speedometer over the temperature interval 1100°C to 800°C.

Lamellar sizes may then be used to calculate a dynamic rate constant for lamellar coarsening. The size data for spinodally-produced lamellae (Table 2) are plotted on a $t^{1/3}$ plot (Fig. 13) and a regression analysis of these data gives the rate constant:

$$\lambda = 70\text{Å} + 107.3 \times t^{1/3}$$

where t is time given in days.

The $t^{1/3}$ law for dynamic coarsening seems to provide an adequate model for lamellar growth in Apollo 15 clinopyroxenes. However, Brady and McCallister (1980) questioned the applicability of a $t^{1/3}$ rate law to coarsening mechanisms in pyroxene. This rate law was derived to treat the coarsening of dispersed spherical particles (Wagner, 1961). When applied to lamellar coarsening the model predicts unreasonably low values of the diffusion coefficient. Also, the simple assumption of lamellar coarsening by diffusion across augite–pigeonite boundaries yields unreasonably low values for the Ca diffusion coefficient (D), when compared to coefficients obtained using other experimental techniques.

Lamellar morphologies in the slowly-cooled clinopyroxenes of Apollo 15 QNBs and in isothermal experiments of Nord and McCallister (in prep.) reveal an alternative mechanism for coarsening. As lamellar wavelength increases (Fig. 10b,d) a bimodal distribution develops. Brady and McCallister suggest that the observed bimodality is consistent with coarsening by selective removal of lamellae to subgrain boundaries leaving a coarser host, and interspaced finer lamellae. Diffusion of Ca from (or to) the lamella that is removed, occurs at the lamella tip where the reduction of the strain field at the curved tip provides the driving mechanism for reduction of surface energy. If coarsening is accomplished by selective removal of lamellae and coarsening of the remaining lamellae, some lamellae may

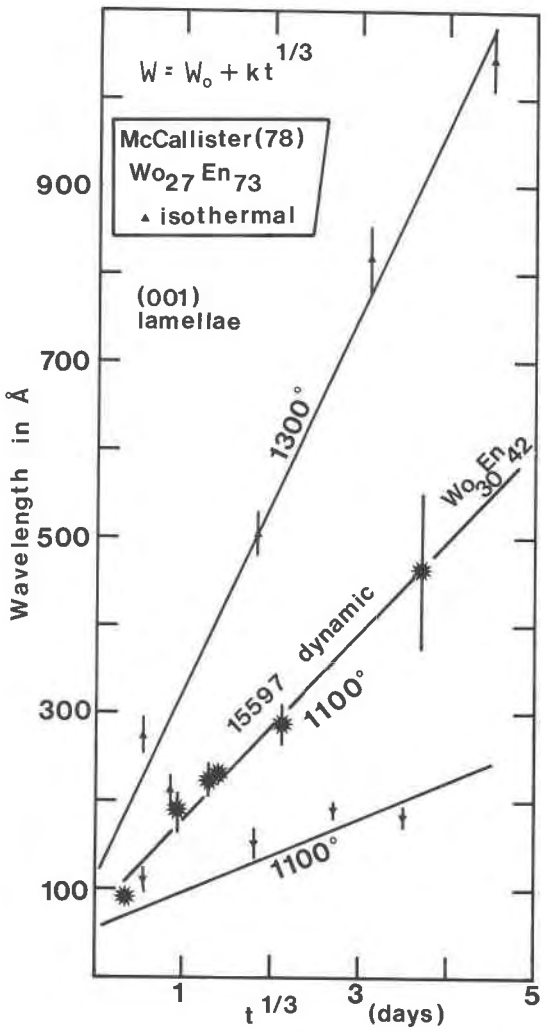

Fig. 13. Wavelength *vs.* $t^{1/3}$ plot for dynamic coarsening of clinopyroxene rims. Stars are data from the 15597 experiments (Table 2). For comparison, the results of isothermal coarsening on a synthetic $Wo_{27}En_{73}$ composition (McCallister, 1978) at 1300° and 1100°C are plotted as triangles. For the QNB experiments W_o = 70.3 and k = 107.3. Correlation coefficient =0.99.

become trapped during their removal. The entrapment occurs when two lamella ends proceeding in opposite directions approach one another. As the tips converge, their strain fields will interact. In order to move past each other the regions near the tip ends must undergo large changes in the sign of the stress field. This stress regime effectively halts lamella removal, and stranded lamella tips are observed in abundance in 15058 (Fig. 10b,d). Thus, a description of coarsening by selective lamella removal must account for the fact that the process stops when two lamellae being removed in opposite directions encounter one another.

Cooling rate speedometry of lunar samples

The dynamic coarsening rates determined from the experimental data may now be used to estimate cooling histories of the lunar samples 15597, 15499 and 15058. In Figure 14 lamellar wavelengths observed in the lunar samples are plotted on the experimentally-determined curve. Care must be taken in applying this estimation technique, and only (001) lamellae produced by the spinodal mechanism must be chosen. Complex textures (Fig. 7a,10) that suggest several exsolution events at different temperatures are not used, but large regions containing regularly-spaced (001) lamellae are assumed to be acceptable.

The integrated cooling rates estimated for the lunar samples are: 15597-20°C/hr., 15499-8°C/hr, 15058-0.02°C/hr. These estimates may now be compared with estimates determined by other techniques and applied to members of the QNB suite. Grove and Walker (1977) used textural criteria to estimate cooling histories of the QNB samples. Their estimates (based on grain sizes) for 15597 and 15499 are similar, though slightly faster for these two lunar samples. Sample 15058's cooling history was estimated using several techniques (Walker *et al.*, 1977). An experimental calibration of plagioclase size *vs.* cooling rate gave 0.1°C/hr integrated over 1050 to 950°C. The cooling rate averaged over 300°C would be ~.03°C/hr, which brings the rate

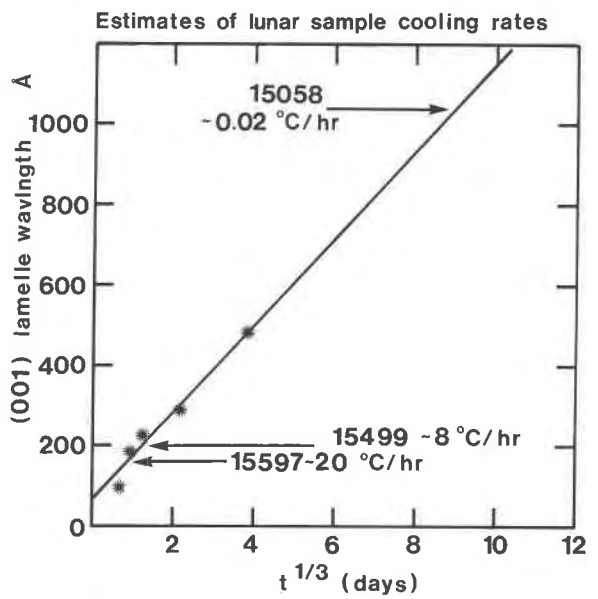

Fig. 14. Estimates of averaged cooling rates for lunar QNB samples 15058, 15499 and 15597.

estimate from plagioclase size and lamellae size into close agreement.

In general, multiple cooling rate speedometers may be used to reconstruct the thermal history of a sample. Jaeger (1957) formalized the suggestion of Winkler (1949) by solving the heat equation for conductive heat loss over a temperature interval. The expression is of the form:

$$v = k/x^2$$

where v is cooling rate, x is distance from a boundary of conductive heat loss, k is a constant which involves the temperature interval over which rate is recorded, the liquidus and solidus temperatures, the thermal diffusivity and latent heat (see Jaeger, 1957, eqn. 13). Plagioclase records rate over the interval 1050° to 950°C and lamellae size records rate from 1100°C to 800°C. These independent rate recorders may be used to solve for the position of a sample from a boundary of conductive heat loss. For 15058 the calculations yield a distance x = 300 cm.

Multiple exsolution textures

The complex multiple exsolution textures observed in regions of heterogeneously-nucleated lamellae (Figs. 7a,c,8a,10a) are strikingly similar to those found in plutonic augites (Robinson *et al.*, 1977). These textures (Fig. 8a) form as a consequence of heterogeneous nucleation of (001) and (100) lamellae on the coherent solvus at an elevated temperature (Fig. 12). Upon further cooling, the low- and high-Ca lamellae enter the coherent spinodal and a second exsolution event produces the shorter wavelength set of lamellae. (The short wavelength lamellae in Figure 8a have $\lambda = 320$Å and the heterogeneous lamellae have $\lambda = 1900$Å for (001) and 1475Å for (100)). Orientations of lamellae in Figure 8a were determined, and the (100) heterogeneous lamellae are oriented −8° from the *c*-axis (using the Robinson *et al.*, 1977 convention). The (001) heterogeneous lamellae span the range of 104° to 106° and the homogeneous (001) lamellae are rotated at an angle of 109° to 111° from *c*. These orientations span the range of values reported for optically visible lamellae in the Bushveld and Kiglapait augites described by Robinson *et al.* The heterogeneous (001) in the QNB pyroxenes are comparable to Stage I of Robinson *et al.* and the homogenous (001) are comparable to Stage II and III in the Bushveld.

Such lamellae orientations are potential indicators of exsolution history and differences in lamellae orientation have been used as estimates of the exsolution temperature. Robinson *et al.* (1977) show that the orientation of lamellar boundaries may be calculated, given a set of pyroxene lattice parameters. Their calculations and estimation technique may be evaluated using the QNB augites, because the temperatures of lamellae formation in the QNB pyroxenes are known.

The multiply-oriented exsolution lamellae were formed before a temperature of 1066°C was reached in 0.5°C/hr cooling rate experiments (Fig. 8a), and the two orientations grow over a much shorter temperature interval (44°C) than would be estimated using the Robinson *et al.* assumptions. If a temperature of 1100°C and reasonable compositions for heterogeneous lamellae are used in the Robinson *et al.* calculation, the observed orientation of (100) and (001) heterogeneous lamellae in the QNB is obtained. However, calculation of lamellae orientations that assume the compositions of homogeneous lamellae determined with the STEM and experimentally reasonable temperatures for the second orientation of (001) do not reproduce the observed orientations. Instead, orientations of homogeneously-nucleated lamellae are similar to within a degree or less to those calculated for heterogeneously-nucleated lamellae.

The solution to the discrepancy in calculated and observed orientations was recognized by Robinson *et al.* (1977). Above the $C2/c \rightarrow P2_1/c$ transition the *a* and *c* cell dimensions of pigeonite are larger than those of augite. However, below the transition temperature the *a* and *c* cell dimensions of pigeonite are smaller than those of augite. The changes are sufficient to produce the observed orientation differences between the (001) heterogeneous and the (001) homogeneous lamellae. Thus, the multiple orientations of pigeonite lamellae in the QNB augites provide a fossil record of the $C2/c$ to $P2_1/c$ transition and bracket the temperature to the interval of 1100° to 1066°C.

The temperature estimates of Robinson *et al.* (1977) may be reevaluated in light of this experimental study. They required a large temperature interval to explain similar orientation differences in Bushveld augites. The calculated temperature for their Stage I exsolution was 1000°C, and Stage II and III were estimated at 800° and 560°C. If their assumed pigeonite lattice parameters were in error, the temperature recorded by each set of lamellae may span a considerably shorter temperature inter-

val, and all may have formed at temperatures in the vicinity of 1100° to 1000°C.

Summary and conclusions

Clinopyroxenes in Apollo 15 QNBs are chemically complex recorders of crystallization history, and the submicroscopic textural variations in augite rims are sensitive indicators of the samples' cooling rate. Variations in wavelength of exsolution lamellae of pigeonite–augite intergrowths produced by spinodal decomposition were experimentally calibrated as a cooling rate speedometer, and used to predict cooling rates of lunar samples. The lamellae form at 1100°C and their coarsening proceeds over the temperature interval 1100–800°C. Previous investigators (Lally *et al.*, 1975; Champness and Lorimer, 1976) predicted the potential usefulness of exsolution textures as indicators of cooling history, and they qualitatively calibrated submicroscopic textures to identify rapidly-cooled *vs.* slowly-cooled samples. Through this experimental calibration of dynamically-coarsened exsolution lamellae, submicroscopic textures may be quantitatively related to average cooling rate.

The observations of QNB augite exsolution lamellae have also shown some of the intricacies that must be dealt with in order to extend a calibration of lamellae size *vs.* cooling history to the slow rates characteristic of plutonic environments. On slow cooling, heterogeneous nucleation on the equilibrium solvus may occur at an elevated temperature. Subsequently the heterogeneously produced lamellae may decompose by a spinodal or nucleation mechanism, producing a complexity of submicroscopic textures over a small temperature interval. TEM observations of exsolution textures in Skaergaard and Bushveld clinopyroxenes indicate the predominance of heterogeneous nucleation (Nakajima and Hafner, 1980; Robinson *et al.*, 1977). These multiple exsolution textures may form over a narrow temperature interval, at the initiation of exsolution, as a consequence of the small temperature difference between the heterogeneous nucleation and homogeneous nucleation.

In using coarsening kinetics as a cooling rate speedometer it is important to know initial temperature of pyroxene growth, and the TTT relation for the pyroxene. Exsolution will be controlled by the crystallization temperature of pyroxene from the magma and by the bulk composition of the pyroxene. The effect of differences in crystallization temperature or bulk composition could require the construction of a new TTT diagram for each clinopyroxene, as the temperature difference between the equilibrium solvus, coherent solvus and coherent spinodal may change significantly for a small compositional change.

Acknowledgments

This research was supported by NSF Grant EAR-7919762. The author thanks A. E. Bence and D. H. Lindsley for support during the early portions of the investigation. The results of this study were presented in the MSA symposium: "Pyroxene Research: Today and Tomorrow" organized by J. Stephen Huebner. The author thanks Bob McCallister and John Brady for interest and stimulating discussions. The thorough reviews of G. L. Nord Jr. and R. A. Yund considerably improved the manuscript.

References

Bence, A. E. and Papike, J. J. (1972) Pyroxenes as recorders of lunar basalt petrogenesis: chemical trends due to crystal-liquid interaction. Proceedings of the 3rd Lunar Science Conference, 431–469.

Brady, J. B. and McCallister, R. H. (1980) Diffusion kinetics of homogenization and coarsening of pigeonite lamellae in subcalcic diopsides. (abstr.) Geological Society of America Abstracts with Programs, 12, 391.

Buseck, P. R., Nord, G. L. Jr., and Veblen, D. R. (1980) Subsolidus phenomena in pyroxenes. In P. H. Ribbe, Ed., Reviews in Mineralogy, V. 7, Pyroxenes, p. 117–211. Mineralogical Society of America, Washington D. C.

Cahn, J. W. (1968) Spinodal decomposition. Transactions of the Metallurgical Society of AIME, 242, 166–180.

Champness, P. E. and Lorimer, G. W. (1976) Exsolution in silicates. In H. R. Wenk, Ed., Electron Microscopy in Mineralogy, p. 174–204. Springer-Verlag, New York.

Christie, J. M., Lally, J. S., Heuer, A. H., Fisher, R. M., Griggs, D. T., and Radcliffe, S. V. (1971) Comparative electron petrography of Apollo 11, Apollo 12 and terrestrial rocks. Proceedings of the 2nd Lunar Science Conference, 69–89.

Cliff, G. and Lorimer, G. W. (1975) The quantitative analysis of thin specimens. Journal of Microscopy, 103, 203–207.

Copley, P. A., Champness, P. E. and Lorimer, G. W. (1974) Electron petrography of exsolution textures in an iron-rich clinopyroxene. Journal of Petrology, 15, 41–57.

Dunham, A. C., Copley, P. A., and Strasser-King, V. H. (1972) Submicroscopic exsolution lamellae in pyroxenes in the Whin Sill, Northern England. Contributions to Mineralogy and Petrology, 37, 211–220.

Grove, T. L. and Bence, A. E. (1977) Experimental study of pyroxene-liquid interaction in quartz-normative basalt 15597. Proceedings of the 8th Lunar Science Conference, 1549–1579.

Grove, T. L. and Raudsepp, M. (1978) Effects of kinetics on the crystallization of quartz-normative basalt 15597: An experimental study. Proceedings of the 9th Lunar and Planetary Science Conference, 585–599.

Grove, T. L. and Walker, D. W. (1977) Cooling histories of Apollo 15 quartz normative basalts. Proceedings of the 8th Lunar Science Conference, 1501–1520.

Hess, H. H. (1960) Stillwater igneous complex, Montana. Geological Society of America Memoir, 80, 230 p.

Huston, E. L., Cahn, J. W., Hilliard, J. E. (1966) Spinodal decomposition during continuous cooling. Acta Metallurgica, 14, 1053–1062.

Jaeger, J. C. (1957) The temperature in the neighborhood of a cooling intrusive sheet. American Journal of Science, 255, 306–318.

Lally, J. S., Heuer, A. H., Nord, G. L. Jr., and Christie, J. M. (1975) Subsolidus reactions in lunar pyroxenes: an electron petrographic study. Contributions to Mineralogy and Petrology, 51, 263–282.

Lofgren, G., Donaldson, C. H., Williams, R. J., Mullins, O. Jr., and Usselman, T. M. (1974) Experimentally reproduced textures and mineral chemistry of Apollo 15 quartz-normative basalts. Proceedings of the 5th Lunar Science Conference, 549–567.

McCallister, R. H. (1978) The coarsening kinetics associated with exsolution in an iron-free clinopyroxene. Contributions to Mineralogy and Petrology, 65, 327–331.

McCallister, R. H. (1980) Determinations of major cation diffusion constants in pyroxenes. (abstr.) Geological Society of America Abstracts with Programs, 12, 479.

McConnell, J. D. C. (1975) Microstructures of minerals as petrogenetic indicators. Annual Reviews of Earth and Planetary Science, 3, 129–155.

Morimoto, N. and Tokonami, M. (1969) Oriented exsolution of augite in pigeonite. American Mineralogist, 54, 1101–1117.

Nakajima, Y. and Hafner, S. S. 1980) Exsolution in augite from the Skaergaard intrusion. Contributions to Mineralogy and Petrology, 72, 101–110.

Nord, G. L. Jr. (1980) Decomposition kinetics in clinopyroxenes. (abstr.) Geological Society of America Abstracts with Programs, 12, 492.

Nord, G. L. Jr., Heuer, A. H., and Lally, J. S. (1976) Pigeonite exsolution from augite. In H.-R. Wenk, Ed., Electron Microscopy in Mineralogy, p 220–227. Springer-Verlag, New York.

Papike, J. J., Bence, A. E., Brown, G. E., Prewitt, C. T., and Wu, C. H. (1971) Apollo 12 clinopyroxenes: Exsolution and epitaxy. Earth and Planetary Science Letters, 10, 307–315.

Putnis, A. and McConnell, J. D. C. (1980) Principles of Mineral Behavior. Elsevier, New York.

Radcliffe, S. V., Heuer, A. H., Fisher, R. M., Christie, J. M., and Griggs, D. T. (1970) High voltage (800kV) electron petrography of Type B rock from Apollo 11. Proceedings of the Apollo 11 Lunar Science Conference, 731–748.

Robinson, P., Jaffe, H. W., Ross, M. and Klein, C. Jr. (1971) Orientation of exsolution lamellae in clinopyroxenes and clinoamphiboles: Consideration of optimal phase boundaries. American Mineralogist, 56, 909–939.

Robinson, P., Ross, M., Nord, G. L. Jr., Smyth, J. R., and Jaffe, H. W. (1977) Exsolution lamellae in augite and pigeonite: Fossil indicators of lattice parameters at high temperature and pressure. American Mineralogist, 62, 857–863.

Ross, M., Huebner, J. S., and Dowty, E. (1973) Delineation of the one atmosphere augite–pigeonite miscibility gap for pyroxenes from lunar basalt 12021. American Mineralogist, 58, 619–635.

Tullis, J. and Yund, R. A. (1979) Calculation of coherent solvi for alkali feldspar, iron-free clinopyroxene, nepheline-kalsilite, and hematite-ilmenite. American Mineralogist, 64, 1063–1074.

Wagner, C. (1961) Theorie der Alterung von Niederschlagen durch Umlösen. Zeitschrift für Elektrochemie, 65, 581–591.

Walker D., Longhi J., Lasaga A. C., Stolper E. M., Grove T. L. and Hays J. F. (1977) Slowly cooled microgabbros 15555 and 15065. Proceedings of the 8th Lunar Conference, 1521–1547.

Winkler, H. G. F. (1949) Crystallization of basaltic magma as recorded by variations of crystal size in dikes. Mineralogical Magazine, 28, 557–574.

Manuscript received, August 12, 1981;
accepted for publication, December 2, 1981.